

The effects of rheological layering on post-seismic deformation

E. A. Hetland* and B. H. Hager

Massachusetts Institute of Technology, Cambridge, MA, USA

Accepted 2006 February 27. Received 2006 February 21; in original form 2005 December 6

SUMMARY

We examine the effects of rheological layering on post-seismic deformation using models of an elastic layer over a viscoelastic layer and a viscoelastic half-space. We extend a general linear viscoelastic theory we have previously proposed to models with two layers over a half-space, although we only consider univiscous Maxwell and biviscous Burgers rheologies. In layered viscoelastic models, there are multiple mechanical timescales of post-seismic deformation; however, not all of these timescales arise as distinct phases of post-seismic relaxation observed at the surface. The surface displacements in layered models with only univiscous, Maxwell viscoelastic rheologies always exhibit one exponential-like phase of relaxation. Layered models containing biviscous rheologies may produce multiple phases of relaxation, where the distinctness of the phases depends on the geometry and the contrast in strengths between the layers. Post-seismic displacements in models with biviscous rheologies can often be described by logarithmic functions.

Key words: post-seismic relaxation, rheological layering, viscoelastic relaxation.

1 INTRODUCTION

Recently, models of multiphase post-seismic relaxation have been proposed to explain observations of post-seismic relaxation that are not adequately described using a single exponential phase of relaxation (e.g. Ivins 1996; Pollitz 2003; Freed & Bürgmann 2004; Montési 2004). Such models incorporate rheologies with more than one component of viscoelastic relaxation, where each distinct phase of surface deformation is assumed to correspond to a different viscosity. These multiviscous rheologies range from linear viscoelastic rheologies containing two viscous relaxation times (e.g. Ivins 1996; Pollitz 2003) to non-linear rheologies with a continuous spectrum of relaxation times (e.g. Freed & Bürgmann 2004; Montési 2004).

In heterogeneous models containing only univiscous Maxwell rheologies, there are multiple timescales in the solutions for post-glacial rebound (e.g. Peltier 1974; Fang & Hager 1995), as well as post-seismic deformation (e.g. Piersanti *et al.* 1995; Ivins & Sammis 1996). In fact, the biviscous relaxation model of Ivins & Sammis (1996) used a composite rheology to represent a random distribution of small regions with a weak Maxwell viscoelastic rheology embedded within a stronger Maxwell viscoelastic material. This biviscous model described the post-seismic deformation observed over 6 months following the 1992 Landers earthquake, where the initial rapid deformation was dominated by stress relaxation in the weak regions, while stress relaxation in the stronger surrounding regions dominated the later deformation (Ivins 1996). While lateral

distributions of materials with differing rheologies are expected in the continental lithosphere (e.g. Rutter & Brodie 1992), variations in the strength of the lithosphere with depth are likely more significant than lateral variations (e.g. Kohlstedt *et al.* 1995). In models of post-seismic relaxation, linear viscoelastic layers of differing strength are commonly used to approximate the depth dependent strength of the lithosphere (e.g. Lyzenga *et al.* 1991; Hager *et al.* 1999; Hetland & Hager 2003; Pollitz 2003). As in models with biviscous rheologies, one may speculate that distinct phases of observed post-seismic relaxation are associated with the viscosities at varying depths in layered models with only Maxwell viscoelastic rheologies.

In this paper, we investigate the effect of rheologic layering on post-seismic deformation at the surface. We consider 2-D models composed of one or two layers overlying a half-space, with a vertical dislocation in the uppermost layer. For brevity we refer to the models with one and two layers over a half-space as one-layer and two-layer models, respectively. We assume that the instantaneous elastic shear modulus is uniform in all of the models that we present in this paper. Many researchers have demonstrated that it is crucial to account for variations in shear moduli in both kinematic and dynamic models (e.g. Rybicki 1971; Chinnery & Jovanovich 1972; Savage 1987; Hager *et al.* 1999; Hearn & Bürgmann 2005); however, in this paper, we wish to isolate the effects of the viscous creep components of the rheologies on the surface deformation. We only consider models with an upper elastic layer and either univiscous Maxwell or biviscous Burgers viscoelastic lower layers. The Maxwell viscoelastic rheology is common in models of crustal deformation (e.g. Rundle & Jackson 1977; Savage & Prescott 1978; Lyzenga *et al.* 1991; Hager *et al.* 1999; Hetland & Hager 2003; Smith & Sandwell 2004). On the other hand, the Burgers rheology has only been used in few

*Now at: Seismological Laboratory, MC 252-21, California Institute of Technology, Pasadena, CA, 91125, USA. E-mail: eheland@alum.mit.edu

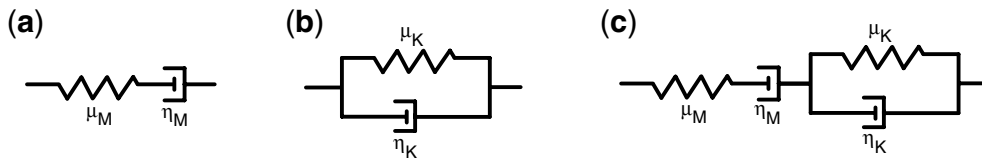


Figure 1. Mechanical analogue models of viscoelastic materials: (a) a Maxwell element, (b) a Kelvin element and (c) a Burgers model.

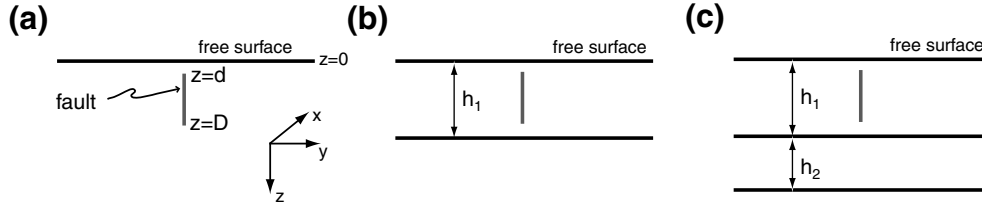


Figure 2. 2-D model geometries considered in this paper: (a) a half-space model, (b) a one-layer model (one layer over a half-space) and (c) a two-layer model (two layers over a half-space). Coordinate system is shown in panel (a).

models of crustal deformation (e.g. Pollitz 2003; Hetland & Hager 2005; Pollitz 2005); however, the Burgers rheology has been used to describe the transient deformation of several geologic materials (e.g. Carter & Ave'Lallemant 1970).

Linear viscoelastic media can be represented by combinations of springs (representing elastic deformation) and dashpots (representing viscous creep) (e.g. Burgers 1939; Flügge 1967). A spring in series (parallel) with a dashpot is a Maxwell (Kelvin) element (Fig. 1). The Maxwell element represents non-recoverable creep, whereas the Kelvin element is fully recoverable and represents delayed elasticity (e.g. Burgers 1939; Flügge 1967). A Maxwell element in series with a Kelvin element is the mechanical analogue of a Burgers viscoelastic rheology, capable of two phases of viscous creep (Fig. 1c) (Burgers 1939). In crustal materials, estimates of the ratio of the Kelvin shear modulus to the Maxwell shear modulus is about 1/3 or less, while the Kelvin viscosity is about 0.1–0.6 times that of the Maxwell viscosity (e.g. Carter & Ave'Lallemant 1970).

Previously, we incorporated general linear viscoelastic rheologies into the interseismic deformation model of Savage & Prescott (1978) (Hetland & Hager 2005). These solutions only hold for models of an elastic layer over a viscoelastic half-space, and in this paper we extend these one-layer models to models of two layers over a half-space. However, as the analytic solutions of this three region geometry is intractable to calculate directly, we use the finite element method to compute post-seismic deformation in two-layer models. Nevertheless, the analytic solutions yield great insight into the nature of the post-seismic deformation in layered models.

2 ANALYTIC MODEL

Displacements due to an infinite length, vertical dislocation extending from $z = d$ to D ($d < D$) in an elastic whole-space are given by

$$u_o(y, z; d, D) = b \cdot v_o(y, z; d, D) \equiv \frac{b}{2\pi} \left[\tan^{-1} \frac{z-d}{y} - \tan^{-1} \frac{z-D}{y} \right], \quad (1)$$

where b is the dislocation, or rupture, offset (e.g. Chinnery 1961; Chinnery & Jovanovich 1972), and for brevity, we take $v_o(d, D) = v_o(y, z; d, D)$. The solution for the displacements in layered models (multiple layers over a half-space) can be constructed from

eq. (1) using the method of images (e.g. Weertman & Weertman 1964; Rybicki 1971; Chinnery & Jovanovich 1972). We define a pair of dislocations reflected about a horizon at depth Z , a so-called image pair, as

$$v(Z) = v(y, z; Z) \equiv v_o(Z + d, Z + D) - v_o(Z - d, Z - D). \quad (2)$$

The displacements due to a dislocation in an elastic half-space (Fig. 2a) are given by the image pair reflected around $Z = 0$

$$u_{hs} = b \cdot v(0) = u_o(d, D) - u_o(-d, -D) \quad (3)$$

(e.g. Chinnery 1961; Chinnery & Jovanovich 1972). In this sign convention for dislocations, $b > 0$ corresponds to a left-lateral fault.

The displacements at the surface due to a dislocation in an elastic layer of thickness h_1 overlying an elastic half-space (a one-layer model; Fig. 2b) are given by image pairs reflected about horizons at depths $Z = 2nh_1$, where n is an index of an infinite sum (Rybicki 1971). The surface displacements due to a dislocation in the upper layer of an elastic two-layer model (two layers over a half-space; Fig. 2c), are given by image pairs reflected about $Z = \pm 2(l + m)h_2 \pm (l + n)h_1$, where l, m , and n are summation indices, and h_1 and h_2 are the thicknesses of the top and middle layers, respectively (Chinnery & Jovanovich 1972). We define

$$W^{+,-}(l, m, n) = W^{+,-}(y, z; l, m, n) \equiv v[\pm 2(l + m)h_2 \pm 2(l + n)h_1] \quad (4)$$

to be the image pairs in both the one- and two-layer models ($W^+ = W^-$ when $z = 0$). The displacements in a layered model depend on these geometric functions as well as the mechanical coupling coefficients between the layers. In the terminology of optics, the coupling coefficients are often described as reflection and transmission coefficients, and depend on the contrast of the shear moduli between the layers (e.g. Chinnery & Jovanovich 1972).

The solution for the time dependent displacements due to the viscoelastic response to a dislocation can be found directly from the elastic solution using the correspondence principle of viscoelasticity (e.g. Flügge 1967), a technique first applied to fault problems by Nur & Mavko (1974). Using the correspondence principle, the viscoelastic solution is obtained by transforming the elastic solution to the Laplace domain, replacing the shear moduli and the rupture offset with the equivalent shear moduli and a fault offset history function, and then transforming back to the time domain. This transformation method has been described in several previous papers (e.g. Nur &

Mavko 1974; Savage & Prescott 1978; Hetland & Hager 2005), and we refer readers to those papers for a detailed discussion.

In the Laplace domain, the reflection and transmission coefficients are

$$\hat{A}_{ij}(s) \equiv \frac{\hat{\mu}_j(s) - \hat{\mu}_i(s)}{\hat{\mu}_j(s) + \hat{\mu}_i(s)} \quad (5)$$

and

$$\hat{B}_{ij}(s) \equiv \frac{2\hat{\mu}_i(s)}{\hat{\mu}_i(s) + \hat{\mu}_j(s)}, \quad (6)$$

where $\hat{\mu}_i(s)$ is the equivalent shear modulus of the material in layer i (g and \hat{g} denote functions of time and the Laplace dual of time, respectively). The equivalent shear moduli of the layers is given by $\hat{\mu}_i(s) = \hat{\Psi}_i(s)/\hat{\Phi}_i(s)$, where $\hat{\Psi}_i(s)$ and $\hat{\Phi}_i(s)$ are Laplace transforms of the stress and strain differential operators in the equation of motion. For linear materials $\hat{\Phi}_i(s)$ and $\hat{\Psi}_i(s)$ are polynomials of s , whose coefficients depend on the shear moduli and viscosities of the viscoelastic material (e.g. Flügge 1967). Throughout this paper we refer to the instantaneous elastic shear modulus and the Maxwell viscosity of layer i as μ_{Mi} and η_{Mi} , respectively, and the Kelvin shear modulus and viscosity as μ_{Ki} and η_{Ki} . The material relaxation times of the Maxwell and Kelvin elements in layer i are then $\tau_{Mi} = \eta_{Mi}/\mu_{Mi}$ and $\tau_{Ki} = \eta_{Ki}/\mu_{Ki}$, respectively.

The reflection and transmission coefficients can be expressed as

$$\hat{A}_{ij}(s) = \frac{\hat{\Phi}_i \hat{\Psi}_j - \hat{\Phi}_j \hat{\Psi}_i}{\hat{\Phi}_i \hat{\Psi}_j + \hat{\Phi}_j \hat{\Psi}_i} \equiv \frac{Q_{ij}(s)}{P_{ij}(s)}, \quad (7)$$

and

$$\hat{B}_{ij}(s) = \frac{2\hat{\Phi}_j \hat{\Psi}_i}{\hat{\Phi}_i \hat{\Psi}_j + \hat{\Phi}_j \hat{\Psi}_i} \equiv \frac{2R_{ij}(s)}{P_{ij}(s)}, \quad (8)$$

and we note that $P_{ij} = P_{ji}$ and $Q_{ij} = -Q_{ji}$. We drop the hat on P , Q , and R since we do not consider them in the time domain, and thus there is no ambiguity over whether they are polynomials in s or functions of t . In the one-layer model of Rybicki (1971) and in the two-layer model of Chinnery & Jovanovich (1972), the reflection and transmission coefficients can be grouped together into

$$\hat{\Gamma}(s; l, m, n) \equiv \hat{A}_{32}^{l+m}(s) \hat{A}_{21}^{m+n}(s) \hat{B}_{12}^l(s) \hat{B}_{21}^n(s). \quad (9)$$

In the time domain, $\Gamma(t; l, m, n)$ completely describes the time dependence due to viscoelastic relaxation following a dislocation in the upper layer.

Based on the elastic solution of Rybicki (1971), the time-dependent surface displacements ($z = 0$) due to a dislocation in a viscoelastic one-layer model are

$$u_1(y, t) = b(t) * \sum_{n=0}^{\infty} \left\{ \begin{array}{l} \Gamma(t; 0, 0, n) W^-(0, 0, n) + \\ \Gamma(t; 0, 0, n+1) W^+(0, 0, n+1) \end{array} \right\}, \quad (10)$$

where $b(t)$ is the fault offset history function, and ‘*’ denotes the convolution operation. For this one-layer model, $\Gamma(t; 0, 0, n) = \hat{A}_{21}^n$, which is referred to as $\Gamma^n(t)$ in Savage & Prescott (1978) and Hetland & Hager (2005). Savage & Prescott (1978) determined $\Gamma^n(t)$ analytically for an elastic layer overlying a Maxwell viscoelastic half-space, while we recently determined $\Gamma^n(t)$ for an elastic layer over any linear viscoelastic half-space (Hetland & Hager 2005). Based on the elastic solution of Chinnery & Jovanovich (1972), the surface displacements in a viscoelastic two-layer model can be found through the addition of a correction term to the one-layer solution:

$$u_2(y, t) = u_1(y, t) + u_C(y, t), \quad (11)$$

where

$$u_C(y, t) = b(t) * \sum_{n=0}^{\infty} \sum_{m=0}^{\infty} \sum_{l=1}^{\infty} (-1)^m \cdot \left\{ \begin{array}{l} \mathcal{B}_{lmn} \Gamma(t; l, m, n) W^+(l, m, n) + \\ \mathcal{A}_{lmn} \cdot \left[\Gamma(t; l, m, n) W^-(l, m, n) + \right. \\ \left. \Gamma(t; l, m, n+1) W^+(l, m, n+1) \right] \end{array} \right\}, \quad (12)$$

$$\mathcal{A}_{lmn} = \frac{(n+l)!(l+m+1)!}{l!n!(l-1)!m!}, \quad (13)$$

and

$$\mathcal{B}_{lmn} = \frac{(n+l-1)!(l+m-1)!}{2(l-1)!n!m!}. \quad (14)$$

The above equations are slightly different than those given by Chinnery & Jovanovich (1972), but can be obtained by algebraic re-ordering of their solution, using the correction noted by Savage (2000).

We use the method introduced by us in Hetland & Hager (2005), to determine $\Gamma(t; l, m, n)$ from eq. (9), as well as its convolution with $b(t)$. Our previous paper was restricted to an upper elastic layer over a viscoelastic half-space, while in this paper, we allow any of the model layers to be either elastic or linear viscoelastic. Eq. (9) is a ratio of polynomials in s , which we re-express as

$$\hat{\Gamma}(s; l, m, n) = 4^l \cdot \frac{Q_{32}^{l+m} Q_{21}^{m+n} R_{12}^l R_{21}^n}{P_{23}^{l+m} P_{12}^{2l+m+n}}. \quad (15)$$

We assume that the polynomials P , Q , and R can be factored, with roots α_k and β_k , as $P_{ij} = \gamma_{P_{ij}} \prod_{k=1}^{\mathcal{N}(P_{ij})} (s - \alpha_k)$ and Q_{ij} , $R_{ij} = \gamma_{Q_{ij}, R_{ij}} \prod_{k=1}^{\mathcal{N}(Q_{ij}, R_{ij})} (s - \beta_k)$, where α_k and β_k are real. We define $\gamma_{P_{ij}}$ to be the leading coefficient of P_{ij} , while we use the notation $\mathcal{N}\{P_{ij}\}$ and $\mathcal{F}\{P_{ij}\}$ to signify the number of roots and the set of roots, respectively, of the polynomial P_{ij} . In a few model rheologies, the realness of the roots can be proved based on the realness of the relaxation moduli of the layers (see Findley *et al.* 1976) for a discussion of viscoelastic relaxation moduli). In this paper we do not attempt a general proof that $\alpha_k \in \mathbb{R}$; however, in our experience we have not encountered linear viscoelastic rheologies resulting in non-real roots, and thus we assert that the roots will always be real as long as the materials are linear and capable of supporting instantaneous shear. Factoring eq. (15) we find

$$\hat{\Gamma}(s; l, m, n) = \gamma \cdot \frac{\prod_{k \in \mathcal{S}_\beta} (s - \beta_k)^{q_k}}{\prod_{k \in \mathcal{S}_\alpha} (s - \alpha_k)^{p_k}}, \quad (16)$$

where \mathcal{S}_α and \mathcal{S}_β are the sets of indices of α_k and β_k , respectively, and

$$\gamma = 4^l \frac{\gamma_{Q_{32}}^{l+m} \gamma_{Q_{21}}^{m+n} \gamma_{R_{12}}^l \gamma_{R_{21}}^n}{\gamma_{P_{23}}^{l+m} \gamma_{P_{12}}^{2l+m+n}}. \quad (17)$$

We use the notation $\alpha_i = \{\alpha_k | k \in \mathcal{S}_\alpha\}$ and $p_i = \{p_k | k \in \mathcal{S}_\alpha\}$, and similarly for β_i and q_i . For elucidation we expand the sets in the denominator of eq. (16):

$$\mathcal{S}_\alpha = [1, \dots, \mathcal{N}\{P_{12}\}, \mathcal{N}\{P_{12}\} + 1, \dots, \mathcal{N}\{P_{12}\} + \mathcal{N}\{P_{23}\}], \quad (18)$$

$$p_k = \begin{cases} (2l + m + n)\kappa_k, & k \in [1, \mathcal{N}\{P_{12}\}] \\ (l + m)\kappa_k, & k \in [\mathcal{N}\{P_{12}\} + 1, \mathcal{N}\{P_{12}\} + \mathcal{N}\{P_{23}\}] \end{cases} \quad (19)$$

and

$$\alpha_k \in \begin{cases} \mathcal{F}\{P_{12}\}, & k \in [1, \mathcal{N}\{P_{12}\}] \\ \mathcal{F}\{P_{23}\}, & k \in [\mathcal{N}\{P_{12}\} + 1, \mathcal{N}\{P_{12}\} + \mathcal{N}\{P_{23}\}] \end{cases} \quad (20)$$

where κ_k is a repeatability index of root α_k .

As in Hetland & Hager (2005), the inverse Laplace transform of eq. (16) is found by partial fraction decomposition (e.g. Churchill 1944; Roberts & Kaufman 1966) and is

$$\Gamma(t; l, m, n) = \gamma \cdot \sum_{k \in S_\alpha} \sum_{j=1}^{p_k} \frac{\Omega_{kj}(\alpha_k, \beta_k; p_k, q_k)}{(p_k - j)!(j - 1)!} t^{p_k - j} e^{\alpha_k t}, \quad (21)$$

where

$$\Omega_{kj} = \sum_{i=0}^{j-1} \binom{j-1}{i} \mathcal{P}_{S_{\alpha/(k)}}^{(i)}(\alpha_k, \alpha_i; p_i) \cdot \mathcal{P}_{S_\beta}^{(j-1-i)}(\alpha_k, \beta_i; q_i) \quad (22)$$

and $\mathcal{P}^{(i)}$ are given by the recursion relation in Hetland & Hager (2005), modified for non-constant powers. Likewise, the convolution $b(t) * \Gamma(t; l, m, n)$ can be found directly from eqs (34)–(36) in Section 2.4 of Hetland & Hager (2005). The timescales in eq. (21) are $|\alpha_k|^{-1}$, which we refer to as mechanical timescales. These mechanical timescales are roots of the denominator of the coupling coefficients, hence $|\alpha_k|^{-1}$ are timescales of the surface relaxation due to the mechanical coupling of layers.

Calculation of u_1 from eq. (10) is quite fast; however, calculation of u_2 from eq. (11) is considerably more difficult as it involves three nested sums. Furthermore, when $q_\alpha > 1$ and the difference between at least two α 's is less than one, calculation of Ω_{kj} is numerically unstable, as it involves division of small numbers raised to positive powers. When $q_\alpha > 1$ and the differences between all α_k are greater than one, division by small numbers is not an issue in the evaluation of Ω_{kj} ; however, the numerical evaluation of eqs (10) and (11) is still not stable because Ω_{k1} grows and alternates for at least one k . In the one-layer model, these instabilities almost always arise well after the solution converges (Hetland & Hager 2005). In the two-layer model, the solution rarely converges before the calculation becomes unstable.

3 MODEL EVALUATION

As explained above, the calculation of the viscoelastic response from a dislocation in a two-layer model is faster and more stable using the finite element method. For this reason, we use the finite element program Adina (Adina R & D) to calculate the displacements in all of the two-layer models. In the instances when we only compare one-layer models to each other, we use the analytic solution of Hetland & Hager (2005). When we compare u_1 to u_2 , we calculate the displacements of the one-layer model using Adina so as to avoid biases due to differences between the finite element method and the analytic solution. In both the analytic and the finite element models we set $d = 0$ and $D = h_1$.

We use a standard finite element model for both u_1 and u_2 . Due to the antisymmetry of an infinite strike-slip fault, we only compute one-half of the model domain. We apply a symmetry boundary condition on the edge containing the fault, set zero displacements along the opposite edge and the bottom of the model domain, and specify the top to be stress free. The finite element model is composed of

three layers: an upper layer of thickness h_1 , a middle layer of thickness h_2 , and a lower layer of thickness $399h_1 - h_2$. The rheologies of the layers are either elastic or linear viscoelastic. At time zero, we prescribe a constant displacement of Δ from the surface to depth h_1 , and linearly taper the displacement to zero at depth $h_1 + h_2/5$. We discretize the $400h_1$ by $400h_1$ model using 12,075 four-node linear quadrilateral elements. We specify a constant node spacing near the fault, and gradually increase the spacing toward the outer edges of the model—the element aspect ratio and gradation are similar to the finite element models used to benchmark the solution of u_1 by Hetland & Hager (2005). We non-dimensionalize time by the Maxwell relaxation time of one of the layers, as discussed below, and we use a constant time step of 1/200 of that Maxwell relaxation time.

4 POST-SEISMIC RELAXATION

In the time dependent displacements, there are at least as many timescales as the number of distinct phases of viscoelastic relaxation. We refer to the timescales $|\alpha_k|^{-1}$ as mechanical timescales, or mechanical relaxation times, in order to distinguish them from the material relaxation times ($\tau = \eta/\mu$, also referred to as viscoelastic relaxation times). When two non-recoverable materials couple, $\hat{\Psi}_i = \hat{\Psi}'_i \cdot s$ for both layers (e.g. Flügge 1967), and thus one of factors of P_{ij} , Q_{ij} , and R_{ij} is zero. There are at least as many ($s - 0$) terms in the numerator as the denominator of eq. (15), so these zero roots cancel and do not appear as infinite time constants in eq. (21).

When eqs (10) and (11) separate into functions that only depend on one of the mechanical timescales (i.e. $u(y, t) = u'(y, \tau_1) + u''(y, \tau_2)$, where $\tau_i = t|\alpha_i|$), we say that the displacements are separable in time and that each separable solution results in a phase of post-seismic surface deformation. The importance of each separable solution varies, as the terms Ω_{k1} and the powers p_k and q_k are not equal in each separable component of the solution (see eq. 21), hence the phases of deformation are not necessarily equally important in the surface displacements. In a two-layer model, when u_1 and u_c are not both separable in time, we say that u_2 is not entirely separable.

Displacements exhibiting a single phase of relaxation can be adequately described by the exponential function

$$u_{\text{exp}} = A(1 - e^{-t/\tau_{\text{exp}}}), \quad (23)$$

(e.g. Savage *et al.* 2003). On the other hand, recent parametrizations of post-seismic displacements have shown that two phases of relaxation are relatively well described by the logarithmic function

$$u_{\text{ln}} = B \ln \left(1 + \frac{t}{\tau_{\text{ln}}} \right) \quad (24)$$

(e.g. Herring 2003; Savage *et al.* 2005). As a rough metric to differentiate between one and two phases of post-seismic relaxation, we introduce the parameter

$$\rho = \frac{E_{\text{exp}} - E_{\text{ln}}}{E_{\text{exp}} + E_{\text{ln}}}, \quad (25)$$

where

$$E_{\text{fun}} = \sqrt{\frac{\sum_{i=1}^N (u_{\text{fun}_i} - u_i)^2}{N}}, \quad (26)$$

and the summation index i is over the discrete times at which the model is evaluated. When $\rho < 0$, the exponential function fits the post-seismic displacements better than the logarithm, roughly indicating a single dominant phase of post-seismic relaxation. Alternatively, when $\rho > 0$, the logarithm describes the displacements better,

indicating two relatively distinct phases of post-seismic relaxation. When $\rho \approx 0$, u_{exp} describe the displacements as well as u_{in} , and the displacements exhibit one prominent phase of relaxation.

In the following subsections, we discuss post-seismic deformation of several one- and two-layer models. For brevity, we refer to the models by the rheologies of the layers. For example, ‘Elastic-Maxwell’ refers to a one-layer model whose upper layer is elastic and the lower half-space is Maxwell viscoelastic, and ‘Elastic-Maxwell-Maxwell’ refers to a two-layer model with an elastic upper layer and a Maxwell viscoelastic middle layer and Maxwell half-space. We assume that the instantaneous elastic shear modulus is identical in all model layers. We non-dimensionalize distance by h_1 and time by one of the Maxwell relaxation times in the model. The material relaxation times are not equal to the mechanical timescales, and thus are not the timescales of the solution for the surface displacements. However, the mechanical timescales are proportional to the Maxwell relaxation times, where the proportionality factors are determined by the contrasts in the viscosities and shear moduli between the layers and between the elements of the rheologies. It is therefore important to note that deformation scales with time only for constant ratios of rheological parameters between the layers and viscoelastic elements (e.g. Hetland & Hager 2005).

4.1 One-layer models

4.1.1 Elastic-Maxwell

In the one-layer model of a vertical fault in an elastic layer overlying a Maxwell half-space, there is only one timescale in eq. (10), and the post-seismic displacements exhibit one phase of relaxation (e.g. Savage & Prescott 1978; Hetland & Hager 2005). The displacements are not given by a single exponential with a time constant equal to the material relaxation of the Maxwell half-space (Fig. 3). Rather, the displacements are given by an infinite sum of exponentials with uniform time constant, decreasing magnitude, and modulated in time (Hetland & Hager 2005). Due to this, there is a slight discrepancy between the surface displacements and the best fit ex-

ponential function, and the exponential coefficients A and τ_{exp} vary with the distance away from the fault (Fig. 3). Moreover, the time constant τ_{exp} is neither the material nor the mechanical relaxation time.

4.1.2 Elastic-Burgers

There are two mechanical timescales, $|\alpha_1|^{-1}$ and $|\alpha_2|^{-1}$, in an Elastic-Burgers model (a fault in an elastic layer overlying a Burgers viscoelastic half-space), and thus $u_1(y, t) = u'_1(y, \tau_1) + u''_1(y, \tau_2)$, where $\tau_i = t|\alpha_i|$ (Hetland & Hager 2005). Since both u'_1 and u''_1 depend only on one timescale, $u_1(y, t)$ is linearly separable in time and there are two phases of relaxation in the post-seismic displacements (Fig. 4a). As the Kelvin element becomes weaker than the Maxwell element, the difference between the two timescales becomes larger and the two phases of post-seismic relaxation are more distinct (Fig. 4). The distinctness of the phases also depends on the ratio of the shear moduli between the Maxwell and Kelvin elements in the Burgers half-space. When $\mu_{K2} \gg \mu_{M2}$ in an Elastic-Burgers model, the post-seismic displacements are those of an Elastic-Maxwell model (Fig. 4).

The displacements resulting from relaxation of coseismic stresses in a Burgers viscoelastic half-space are not described by a single exponential, rather the displacements can be adequately described using a logarithmic function (Figs 5 and 6). When $\mu_{K2} = \mu_{M2}/3$ and $\eta_{K2} = \eta_{M2}(\tau_{K2} = 3\tau_{M2})$, the displacements are fit by a logarithmic function better than an exponential (Fig. 5); however, the two phases are not as distinct as when $\eta_{K2} < \eta_{M2}$. The logarithmic time constant is neither the mechanical nor any of the material relaxation times (Fig. 6d). The relative fits of u_{exp} and u_{in} depend on the time window over which the displacements are considered. For example, when the displacements from an Elastic-Burgers model with $\eta_{K2} = \eta_{M2}$ and $\mu_{K2} = \mu_{M2}/3$ (Fig. 5b), are considered over $15\tau_{M2}$, as opposed to $30\tau_{M2}$, ρ changes from 0.24 to -0.31 , indicating that only one phase of relaxation is dominant in this shorter time window. Likewise, ρ of the Elastic-Maxwell model shown in Fig. 5(a) drops from -0.49 to -0.69 when only considered over the first $15\tau_{M2}$, indicating that

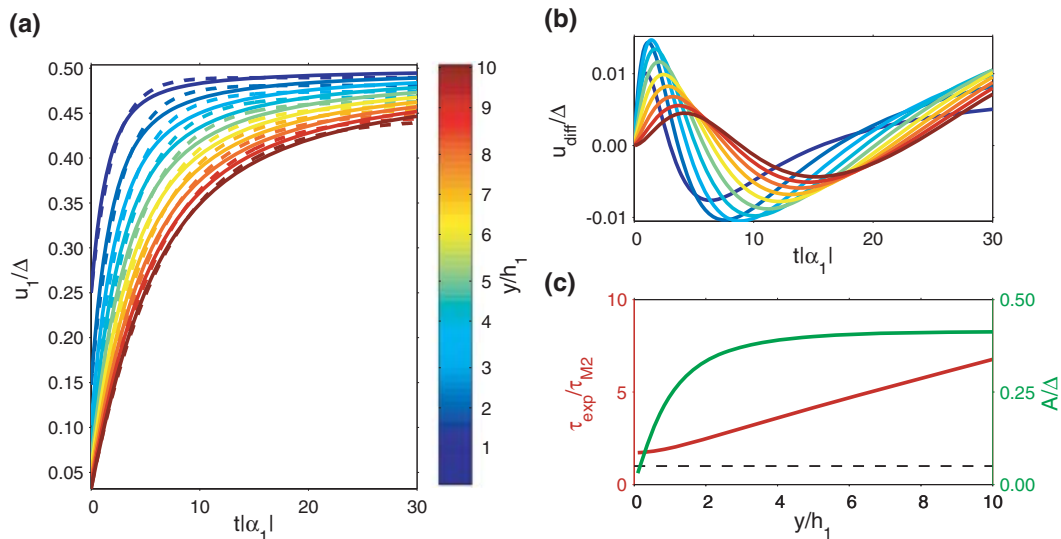


Figure 3. (a) Post-seismic surface displacements in an Elastic-Maxwell model (u_1 ; solid lines) and exponential functions fit to the displacements (u_{exp} ; dashed lines). (b) Difference between the surface displacements and the best fit exponential ($u_{\text{diff}} = u_1 - u_{\text{exp}}$). (c) The variation of the parameters of u_{exp} with distance from the fault, black dashed line is $|\alpha_1|^{-1} = 2\tau_{M2}$.

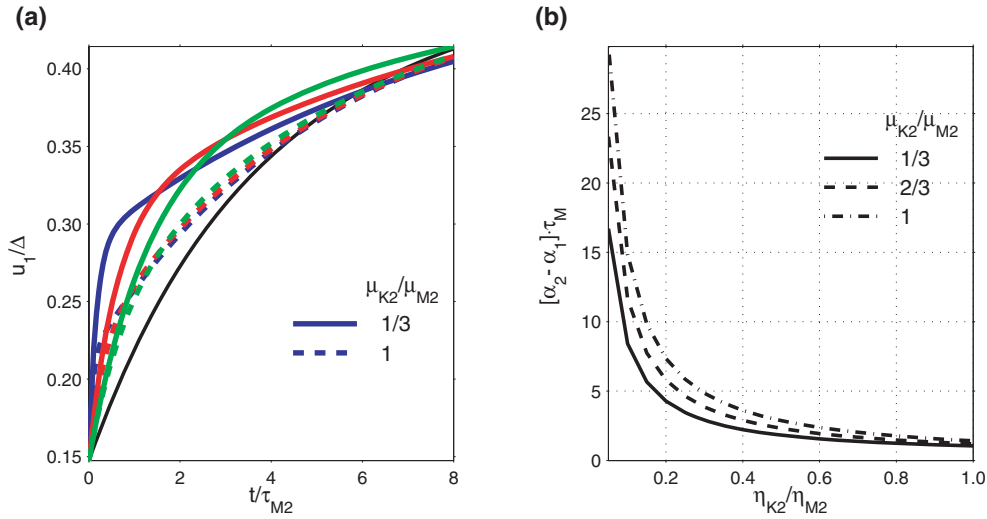


Figure 4. (a) Post-seismic displacements $2h_1$ from the fault in an Elastic-Burgers model, with $\eta_{K2} = \eta_{M2}/10$ (blue lines), $\eta_{K2} = 2\eta_{M2}/5$ (red lines), $\eta_{K2} = \eta_{M2}$ (green lines), also shown are the displacements in an Elastic-Maxwell model (black line). (b) The difference between the two mechanical timescales in an Elastic-Burgers model with $\mu_{K2} = \mu_{M2}/3$ (solid line), $2\mu_{M2}/3$ (dashed line), and μ_{M2} (dash-dot line).

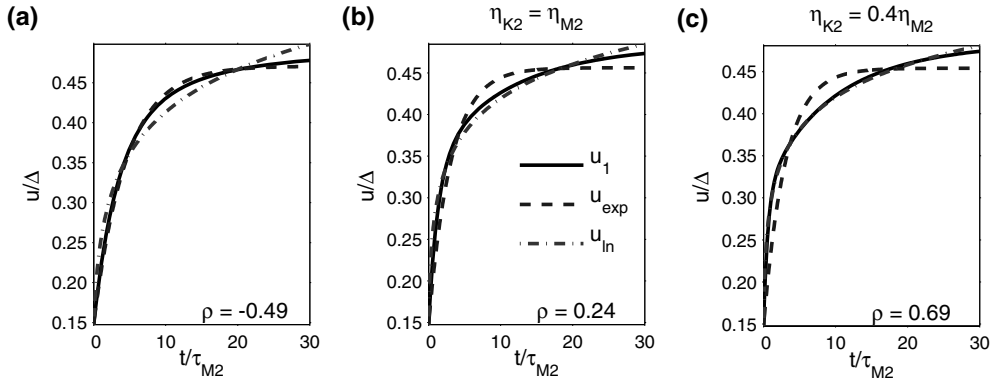


Figure 5. Post-seismic surface displacements (u_1 ; solid lines) $2h_1$ from faults in an Elastic-Maxwell model (a), and Elastic-Burgers models ($\mu_{K2} = \mu_{M2}/3$) with $\eta_{K2} = \eta_{M2}$ (b) and $\eta_{K2} = 0.4\eta_{M2}$ (c). Also shown are the best fit exponential (u_{exp} ; dashed lines) and logarithmic (u_{ln} ; dash-dot lines) functions.

the perturbations from a single exponential in u_1 are less important in early times.

4.2 Two-layer solution

4.2.1 Elastic-Maxwell-Maxwell

For a two-layer model of a fault in an elastic upper layer over a Maxwell viscoelastic layer ($\tau_{M2} = \eta_{M2}/\mu$, μ is the shear modulus of the entire model) and a Maxwell half-space ($\tau_{M3} = \eta_{M3}/\mu$), $\hat{\Gamma}(s)$ reduces to

$$\hat{\Gamma}(s; l, m, n) = \gamma \cdot \frac{\left(s + \frac{\eta_{M3} - \eta_{M2}}{\eta_{M3}\tau_{M2} + \eta_{M2}\tau_{M3}}\right)^{l+m} \left(s + \frac{1}{\tau_{M2}}\right)^l s^l}{\left(s + \frac{\eta_{M3} + \eta_{M2}}{\eta_{M3}\tau_{M2} + \eta_{M2}\tau_{M3}}\right)^{l+m} \left(s + \frac{1}{2\tau_{M2}}\right)^{2l+m+n}}, \quad (27)$$

where $\gamma = 4^l \left(\frac{\eta_{M3}\tau_{M2} - \eta_{M2}\tau_{M3}}{\eta_{M3}\tau_{M2} + \eta_{M2}\tau_{M3}}\right)^{l+m} \left(\frac{1}{2\tau_{M2}}\right)^{m+n}$, and we identify $\alpha_1 = -1/2\tau_{M2}$ and $\alpha_2 = -(\eta_{M2} + \eta_{M3})/(\eta_{M3}\tau_{M2} + \eta_{M2}\tau_{M3})$. We then

write eq. (21) as

$$\Gamma(t; l, m, n) = \gamma \cdot \left[\sum_{j=1}^{2l+m+n} \frac{\Omega_{1j}}{(2l+m+n-j)!(j-1)!} t^{2l+m+n-j} e^{t\alpha_1} + \sum_{j=1}^{l+m} \frac{\Omega_{2j}}{(l+m-j)!(j-1)!} t^{l+m-j} e^{t\alpha_2} \right]. \quad (28)$$

In general, for an Elastic-Maxwell-Maxwell model, $P_{12} = \gamma p_{12}(s - \alpha_1)$ and $P_{23} = \gamma p_{23}(s - \alpha_2)s$. The s term in P_{23} cancels due to the zero root in Q_{32} , leaving two mechanical timescales of u_2 , $|\alpha_1|^{-1}$ and $|\alpha_2|^{-1}$, associated with the coupling of the upper two layers and the middle layer with the lower half-space, respectively. The coupling coefficients are

$$\alpha_1 = -\frac{\chi_1}{(1 + \chi_1)\tau_{M2}}, \quad (29)$$

and

$$\alpha_2 = -\frac{1 + \chi_2\xi}{(1 + \chi_2)\xi}\frac{1}{\tau_{M2}}, \quad (30)$$

where $\chi_1 = \mu_{M1}/\mu_{M2}$, $\chi_2 = \mu_{M3}/\mu_{M2}$, $\xi = \tau_{M3}/\tau_{M2}$. Since $|\alpha_2|^{-1}$ is a timescale of the displacements at the surface, it cannot be expressed as dependent only on χ_2 , ξ , and τ_{M3} , and thus $|\alpha_2|^{-1}$ only

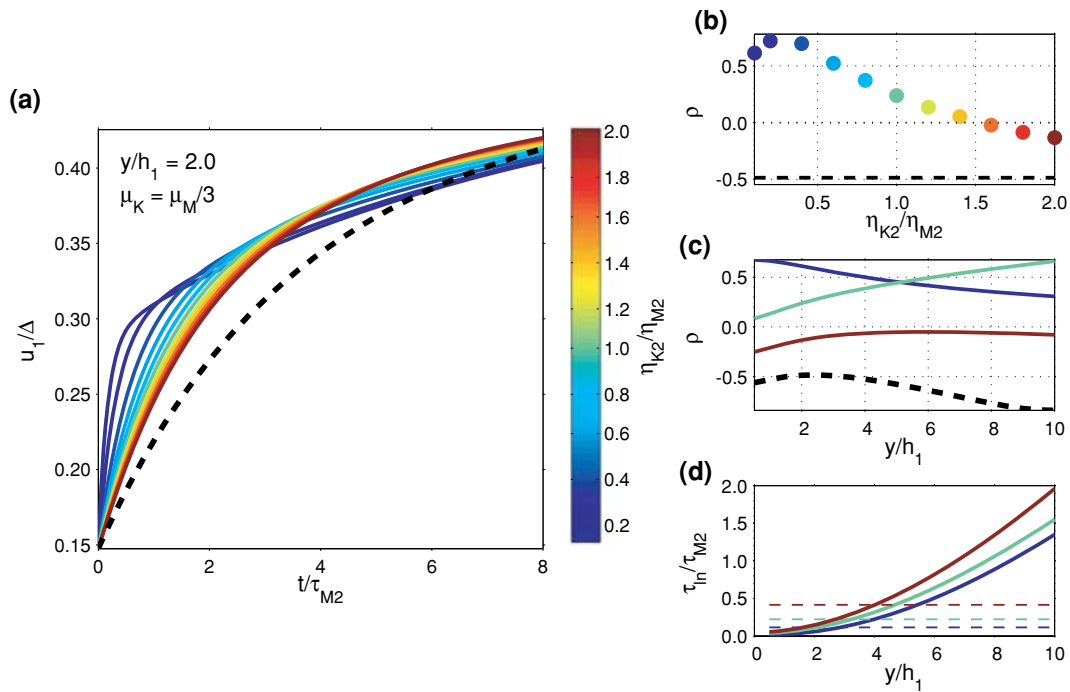


Figure 6. (a) Post-seismic displacements $2h_1$ from the fault in an Elastic-Maxwell (black dashed line) and Elastic-Burgers ($\mu_{K2} = \mu_{M2}/3$; solid lines) models. (b) ρ as a function of the ratio of the Maxwell to Kelvin viscosities; dashed black line is ρ for the Elastic-Maxwell model. (c) ρ as a function of distance from the fault in an Elastic-Maxwell model (dashed line) and Elastic-Burgers models with $\eta_{K2}/\eta_{M2} = 0.1$ (blue line; shading is as in colour scale at left), 1.0 (green line), and 2.0 (red line). (d) Time constant of the best fit logarithm (solid lines, line colour is as in panel c) and the fastest mechanical timescales for each model shown (dashed lines).

scales with τ_{M2} for constant χ_2 and ξ . Eq. (21) decomposes into $\Gamma(t; 0, 0, n) \sim e^{\alpha_1 t}$ and $\Gamma(t; l, m > 0, n) \sim e^{\alpha_1 t} + e^{\alpha_2 t}$. Defining $\tau_i = |\alpha_i|t$, the surface displacements can be written as

$$u_2(y, t) = u'_1(y, \tau_1) + u'_C(y, \tau_1) + u''_C(y, \tau_2). \quad (31)$$

The correction term in eq. (12) is separable in time, but the leading half-space term is only a function of α_1 . The component u''_C only includes a sum to $m + n$ inside eq. (11), while u'_C includes an additional summation to $2l + m + n$.

As the material relaxation time of the middle layer becomes very large, the surface displacements in the Elastic-Maxwell-Maxwell model approach those of an Elastic-Maxwell model with $D = h_1$ and an elastic layer thickness of $h_1 + h_2$, and are a function of α_2 only. On the other hand, when the material relaxation time of the half-space is much longer than the middle layer, relaxation in the middle layer dominates the surface displacements, and thus u_2 is only a function of α_1 . In both of these limits, the displacements are characterized by a single phase of relaxation; however, u_2 is not entirely separable, and thus between these limits there is also only one dominant phase of relaxation (Fig. 7).

The displacements in an Elastic-Maxwell-Maxwell model are fit adequately by an exponential function (Figs 7 and 8). The metric ρ is close to zero when $\eta_{M3} > \eta_{M2}$, indicating that both u_{exp} and u_{in} fit the deformation about as well near the fault and that there is only one dominant phase of relaxation visible over the first $30\tau_{M2}$ (Figs 7a and 8). That ρ is zero far from the fault when $\eta_{M3} > \eta_{M2}$ is because we only considered the displacements over the first $30\tau_{M2}$ and the displacements are small in the far-field (Fig. 8). When $\eta_{M3} < \eta_{M2}$, ρ is always less than zero, similar to an Elastic-Maxwell model (Fig. 8c).

When the middle layer is much weaker than the lower half-space, coseismic stress relaxation is almost entirely within the middle layer,

producing short wavelength deformation near the fault (Fig. 9). On the other hand, when the half-space is weaker than the middle layer, the relaxation in the half-space dominates that in the middle layer and the post-seismic deformation at the surface is long-wavelength (Fig. 9). The time constant in the best fit u_{exp} depends on both α_1 and α_2 , and τ_{exp} and A of u_{exp} vary with the distance from the fault (Figs 7b–d). When $\eta_{M3} < \eta_{M2}$ (i.e. long wavelength deformation), the parameters of u_{exp} vary slowly with distance, whereas, when the deformation is short wavelength, A and τ_{exp} vary widely (Fig. 7). When $\eta_{M3} = \eta_{M2}/10$, the exponential time constant is near to the mechanical timescale (Fig. 7b); however, this is a particular case.

The post-seismic displacements of an Elastic-Maxwell-Maxwell model can be described using those of an Elastic-Maxwell model. Both the apparent mechanical timescale (τ^*) and the amplitude (Δ^*) of the Elastic-Maxwell model fit to the Elastic-Maxwell-Maxwell model depend on distance, because the wavelengths of deformation are highly variable for differing η_{M3}/η_{M2} (Figs 9 and 10). For instance, the post-seismic displacements close to the fault in an Elastic-Maxwell-Maxwell model with $\eta_{M3} = \eta_{M2}/10$ can be described using an Elastic-Maxwell model with $\tau^* \approx \tau_{M2}/2$, while at larger distances a slightly shorter timescale (i.e. weaker half-space) is required (Fig. 10). For an Elastic-Maxwell-Maxwell model with $\eta_{M3} = 10\eta_{M2}$, the displacements close to the fault are similar to those of an Elastic-Maxwell model with $\tau_{M2} < \tau^* < 2\tau_{M2}$, while τ^* increases away from the fault. However, at distances less than about $5h_1$ from the fault, τ^* of the Elastic-Maxwell model is less than an order of magnitude greater than the relaxation time of the middle layer. In general, the mapping between the mechanical relaxation time of a one-layer model and the relaxation times in a two-layer model depends on η_{M2}/η_{M3} , the shear moduli, and the layer thicknesses, and we have only presented

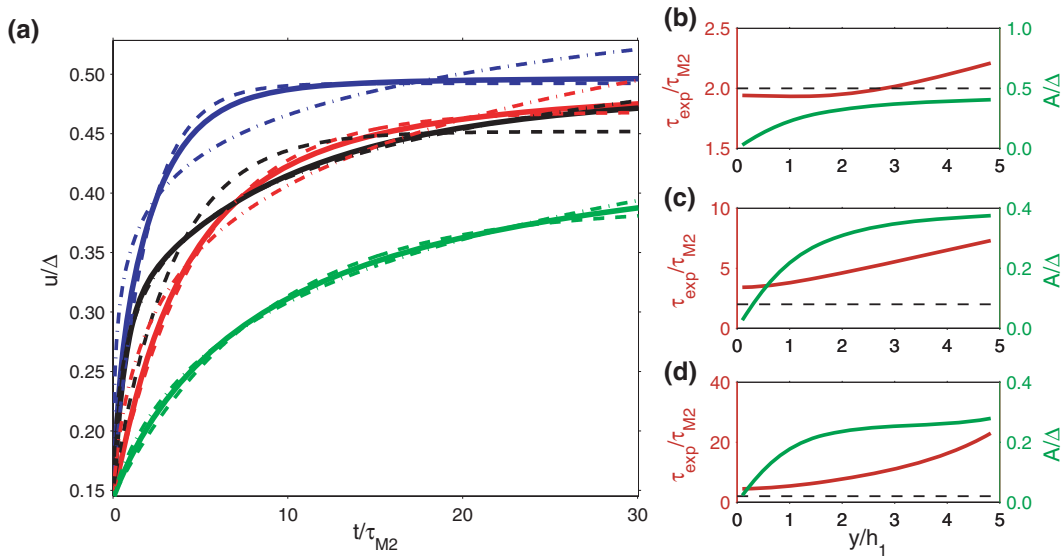


Figure 7. (a) Post-seismic displacements $2h_1$ from the fault in an Elastic-Burgers model ($\mu_{K2} = \mu_{M2}/3$, $\eta_{K2} = 0.4\eta_{M2}$; black solid line) and Elastic-Maxwell models ($h_1 = h_2$) with $\eta_{M3} = \eta_{M2}/10$ (blue solid line), $\eta_{M3} = \eta_{M2}$ (red solid line), and $\eta_{M3} = 100\eta_{M2}$ (green solid line), shown with the best fit exponential (dashed lines) and logarithmic (dash-dot lines) functions. (b)–(d) The variation of the best fit exponential parameters with distance from the fault in an Elastic-Maxwell model with $\eta_{M3} = \eta_{M2}/10$ (b), $\eta_{M3} = \eta_{M2}$ (c), and $\eta_{M3} = 100\eta_{M2}$ (d).

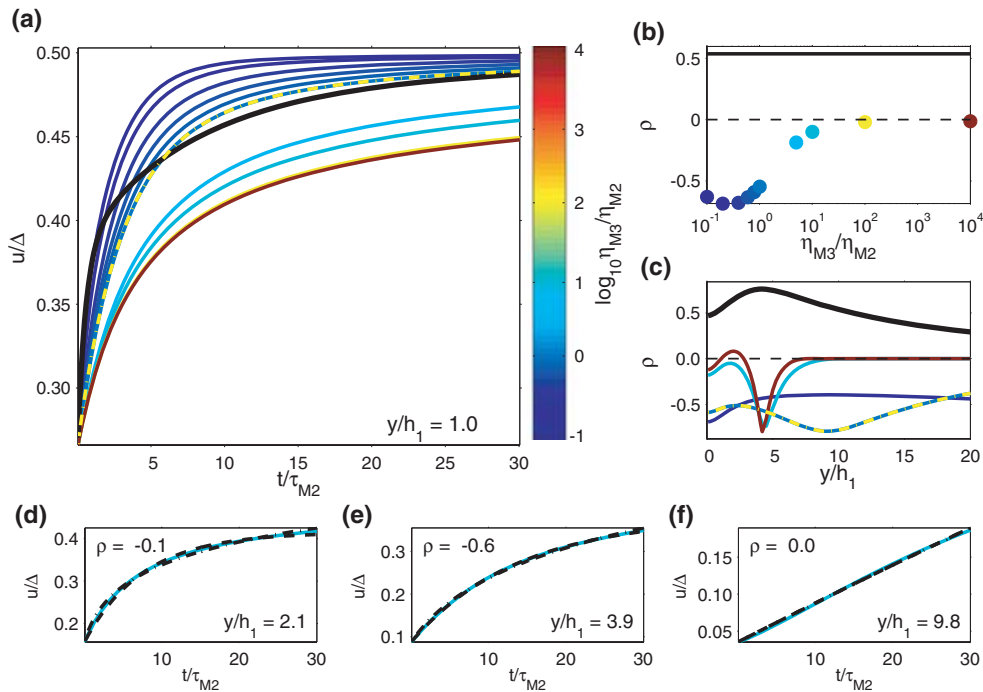


Figure 8. (a) Post-seismic displacements in an Elastic-Maxwell-Maxwell model ($h_1 = h_2$; coloured solid lines), an Elastic-Maxwell model (yellow dash-dot line) and an Elastic-Burgers model ($\mu_{K3} = \mu_{M3}/3$, $\eta_{K3} = 0.4 \cdot \eta_{M3}$; black line), all with uniform elastic shear modulus. (b) ρ as a function of the viscosity contrast in the Elastic-Maxwell-Maxwell models, solid line is ρ for the Elastic-Burgers model, and dashed line is $\rho = 0$. (c) ρ for several models in panel (a) as a function of distance from the fault. (d)–(f) Displacements in an Elastic-Maxwell-Maxwell model with $\eta_{M3}/\eta_{M2} = 10$ (cyan solid lines) and the best fit exponential (black dashed line) and logarithmic (black dash-dot lines) functions.

one combination of layer thicknesses and elastic shear moduli for demonstration.

4.2.2 Elastic-Maxwell-Burgers

For a fault in an elastic layer over a Maxwell middle layer and a Burgers viscoelastic half-space (an Elastic-Maxwell-Burgers model),

$P_{12} = \gamma_{P_{12}}(s - \alpha_1)$ and $P_{23} = \gamma_{P_{23}}(s - \alpha_2)(s - \alpha_3)s$. As before, the zero root in P_{23} cancels, and there are three timescales of u_2 ; however, under some circumstances, one of the mechanical timescales due to the coupling of the middle layer with the lower half-space is identical to the timescale due to the coupling of the upper two layers (Fig. 11). In general, eq. (21) decomposes into $\Gamma(t; 0, 0, n) \sim e^{\alpha_1 t}$ and $\Gamma(t; l, m > 0, n) \sim e^{\alpha_1 t} + e^{\alpha_2 t} + e^{\alpha_3 t}$, so

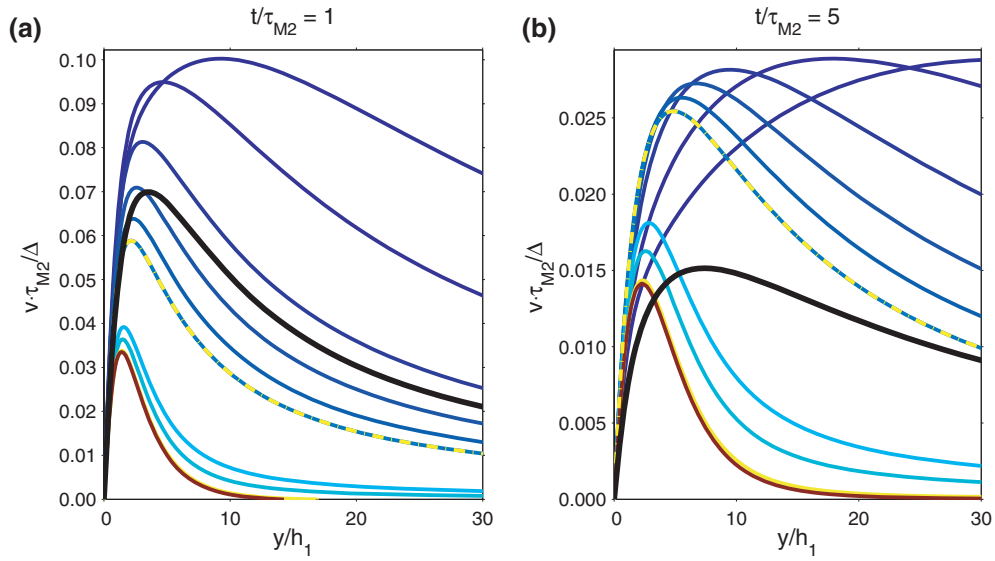


Figure 9. Post-seismic velocities at τ_{M2} (a) and $5\tau_{M2}$ (b) after the earthquake in the models shown in Fig. 8.

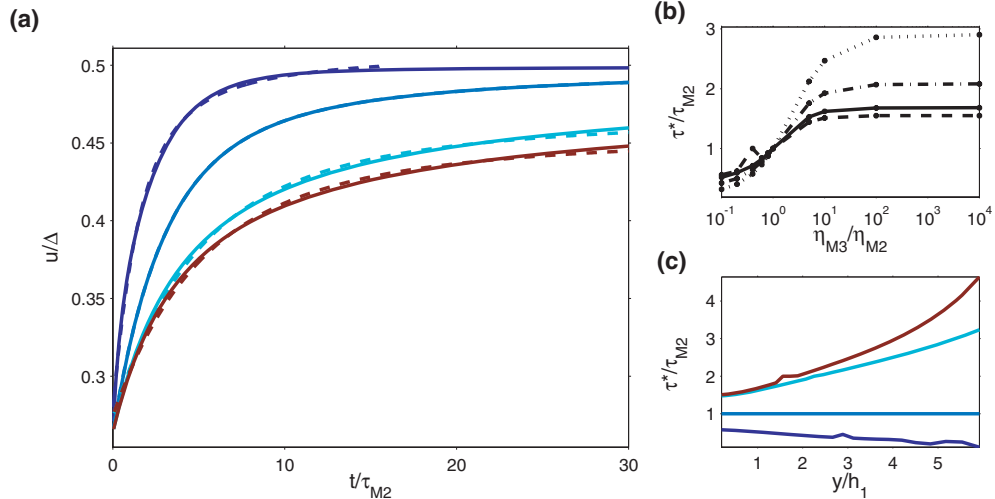


Figure 10. (a) Post-seismic displacements h_1 from the fault in an Elastic-Maxwell-Maxwell model ($h_1 = h_2$; solid lines) and Elastic-Maxwell models (dashed lines) that best fit the two-layer models; line type is as in Fig. 8. (b) The effective Maxwell relaxation time (τ^*) of the best fit Elastic-Maxwell models as a function of η_{M3}/η_{M2} at $y/h_1 = 0.5$ (dashed line), 1.0 (solid line), 2.0 (dash-dot line) and 4.0 (dotted line). (c) τ^* as a function of distance from the fault.

that for $\tau_i = |\alpha_i|t$,

$$u_2(y, t) = u'_1(y, \tau_1) + u'_c(y, \tau_1) + u''_c(y, \tau_2) + u'''_c(y, \tau_3). \quad (32)$$

As for the Elastic-Maxwell-Maxwell model, the solution is not entirely separable in time.

When the Maxwell relaxation time of the middle layer is much larger than the material relaxation times of the half-space, the surface displacements approach those of a one-layer model with $D = h_1$ and an upper elastic layer of thickness $h_1 + h_2$. In this limit, $u'_1(y, \tau_1), u'_c(y, \tau_1) \rightarrow 0$ since the timescale due to the coupling of the upper layer with the middle layer is larger than the timescales due to the coupling of the middle layer with the lower half-space (Fig. 11). When $\eta_{M2} > \eta_{M3}$, the solution becomes separable in time, as $u \rightarrow u''_c(\tau_2) + u'''_c(\tau_3)$, and the displacements are always described by a logarithm better than a single exponential (Fig. 12).

When the middle layer is weaker than the half-space, the post-seismic displacements near the fault mainly reflect relaxation in the middle layer and can be described slightly better by an exponential function than a logarithm (Fig. 12). However, the displacements farther from the fault are fit better by u_{ln} , indicating that they reflect the biviscous rheology in the lower half-space (Fig. 12). When $h_1 = h_2$ and $\eta_{M2} = \eta_{M3}/10$, the displacements are similar to an Elastic-Maxwell-Maxwell model close to the fault, while at greater distances the displacements are similar to an Elastic-Burgers model (Figs 12a and b). The far-field post-seismic velocities are larger than those from an Elastic-Maxwell-Maxwell model with a weak middle layer, further indicating that substantial post-seismic deformation occurs in the lower half-space of the Elastic-Maxwell-Burgers model compared to the Elastic-Maxwell-Maxwell model (Fig. 13).

As the thickness of the middle layer decreases, the two phases of relaxation become more distinguishable in the surface displacements and the model approaches an Elastic-Burgers model

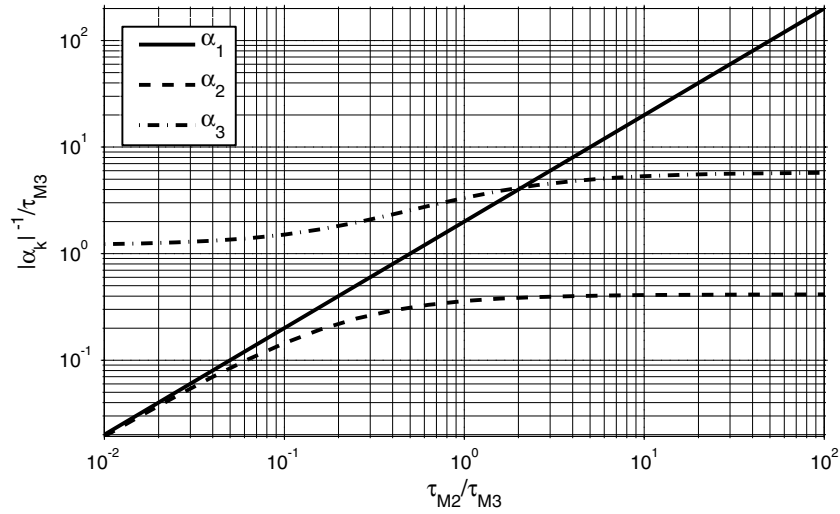


Figure 11. Mechanical timescales of the Elastic-Maxwell-Burgers model with uniform shear modulus; α_1 is a root of P_{12} , whereas α_2 and α_3 are roots of P_{23} .

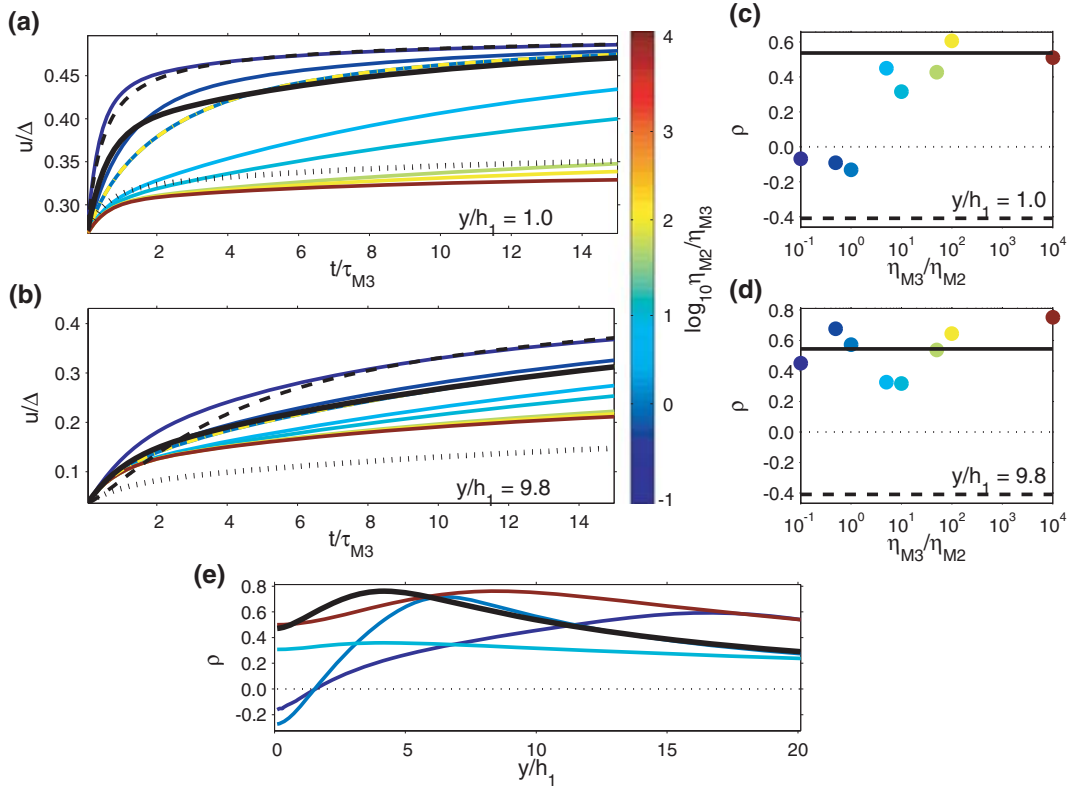


Figure 12. (a) and (b) Post-seismic displacements in an Elastic-Maxwell-Burgers model ($h_1 = h_2$; coloured solid lines), an Elastic-Maxwell model ($\eta_{M3} = 10\eta_{M2}$; black dashed line), and an Elastic-Burgers model ($\mu_K = \mu_{M3}/3$, $\eta_{K3} = 0.4\eta_{M3}$; thick black line); also shown is the Elastic-Burgers model arbitrarily rescaled (black dotted line). (c) and (d) ρ for the displacements in panel (a) (c) and (b) (d); coloured dots correspond to η_{M2}/η_{M3} in the Elastic-Maxwell-Burgers models, and black solid and dashed lines are ρ of the Elastic-Burgers and Elastic-Maxwell models shown at left, respectively. (e) ρ with distance from the fault for an Elastic-Burgers model (black line) and for Elastic-Maxwell-Burgers models with $\eta_{M3}/\eta_{M2} = 0.1$ (dark blue line; colour corresponds to colour scale in a), 1.0 (blue line), 10 (cyan line) and 10^4 (red line).

(Fig. 14a). The number of phases of relaxation at the surface also depends on the distance from the fault, and far from the fault the displacements are more sensitive to the biviscous rheology of the lower half-space. The distance at which $\rho \approx 0$ scales with h_1/h_2 , and when $h_1 > 2h_2$ the displacements are always described by a logarithmic function better than an exponential (Fig. 14b).

4.2.3 Elastic-Burgers-Maxwell

For a fault in an elastic layer overlaying a Burgers viscoelastic layer and a Maxwell viscoelastic half-space there are four mechanical timescales: two resulting from the coupling between the upper two layers, $P_{12} = \gamma_{P_{12}}(s - \alpha_1)(s - \alpha_2)$, and two from the coupling

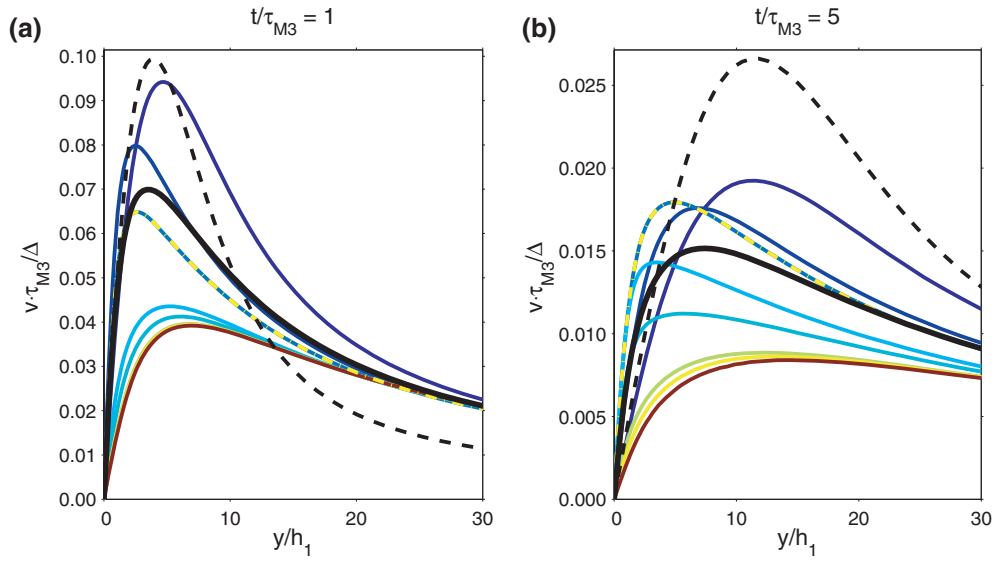


Figure 13. Post-seismic velocities τ_{M3} (a) and $5\tau_{M3}$ (b) after a rupture for the models in Fig. 12.

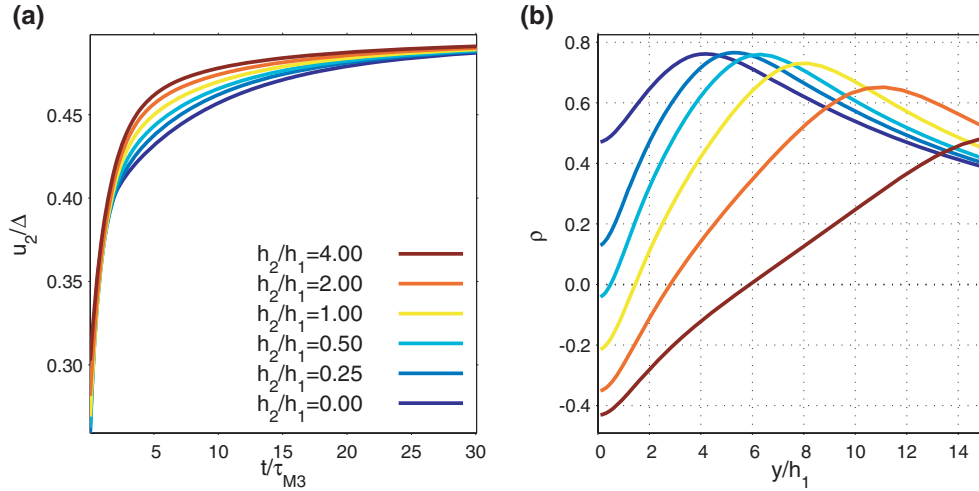


Figure 14. (a) Post-seismic displacements $2h_1$ from the fault in Elastic-Maxwell-Burgers models with various h_2/h_1 . (b) ρ for each h_1/h_2 as a function of distance from the fault.

of the middle layer and lower half-space, $P_{23} = \gamma P_{23}(s - \alpha_3)(s - \alpha_4)s$ (the zero root cancels and does not appear as a mechanical timescale). Eq. (21) decomposes into $\Gamma(t; 0, 0, n) \sim e^{\alpha_1 t} + e^{\alpha_2 t}$ and $\Gamma(t; l, m > 0, n) \sim e^{\alpha_1 t} + e^{\alpha_2 t} + e^{\alpha_3 t} + e^{\alpha_4 t}$, so that for $\tau_i = |\alpha_i|t$,

$$u_2(y, t) = u'_1(y, \tau_1) + u'_C(y, \tau_1) + \quad (33)$$

$$u''_1(y, \tau_2) + u''_C(y, \tau_2) + u'''_C(y, \tau_3) + u'''_C(y, \tau_4), \quad (34)$$

which can be grouped as

$$u_2(y, t) = u'_2(y, \tau_1) + u''_2(y, \tau_2) + u'''_C(y, \tau_3) + u'''_C(y, \tau_4). \quad (35)$$

Hence, the solution is separable with respect to α_1 and α_2 (the roots associated with the coupling of the elastic layer to the Burgers layer), while only the correction term depends on α_3 and α_4 .

The initial transient deformation associated with the Kelvin element in the middle layer is localized near the fault (Fig. 15). Far

from the fault, the transient Kelvin relaxation is not apparent and the steady deformation of the Maxwell elements of the middle layer and lower half-space dominates. The steady deformation in the far-field, as well as late in time, is similar to the deformation from an Elastic-Maxwell-Maxwell model, as the transient Kelvin stress relaxation is confined to the thin middle layer (Figs 15 and 16). In fact, when the Burgers rheology is confined to the middle-layer, $\rho > 0$ close to the fault, while at larger distances an exponential function fits the deformation adequately (Fig. 17). On the other hand, when the Burgers rheology is only in the lower half-space, the near-field deformation is exponential-like, while away from the fault the deformation exhibits the two phases of relaxation captured by u_{in} (Fig. 17).

4.2.4 Elastic-Burgers-Burgers

For a fault in an upper elastic layer overlying a viscoelastic middle layer and lower half-space both with Burgers rheologies (an Elastic-Burgers-Burgers model), there are five mechanical timescales in

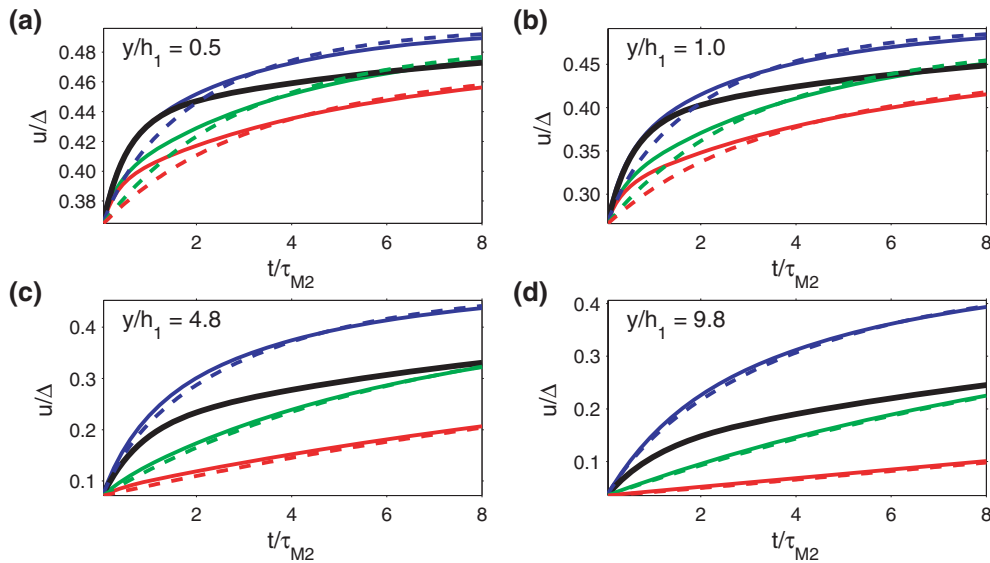


Figure 15. Post-seismic displacements in an Elastic-Burgers-Maxwell model ($h_1 = h_2$, $\mu_{K2} = \mu_{M2}/3$, and $\eta_{K2} = 0.4\eta_{M2}$) with $\eta_{M3} = \eta_{M2}/5$ (blue line), $\eta_{M3} = \eta_{M2}$ (green line) and $\eta_{M3} = 5\eta_{M2}$ (red line) with those from an Elastic-Burgers model ($\mu_{K2} = \mu_{M2}/3$ and $\eta_{K2} = 0.4\eta_{M2}$; black line) and an Elastic-Maxwell-Maxwell model ($\eta_{M3} = \eta_{M2}/5$; blue dashed line), $\eta_{M3} = \eta_{M2}$ (green dashed line), and $\eta_{M3} = 5\eta_{M2}$ (red dashed line).

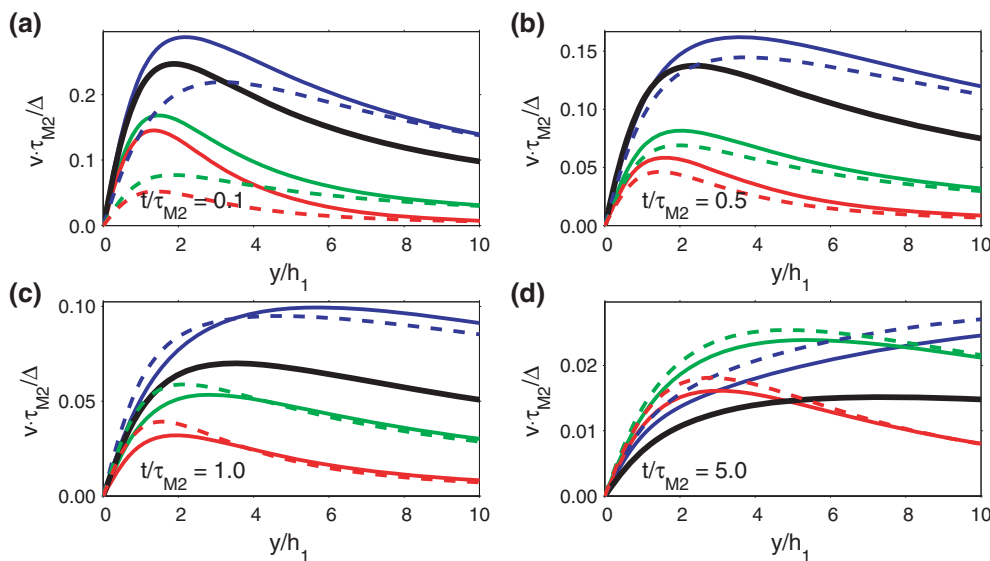


Figure 16. Post-seismic velocities in an Elastic-Burgers-Maxwell model; parameters and line-style is as in Fig. 15.

the solution for the displacements. Two timescales arise from the coupling of the upper elastic layer with the Burgers viscoelastic middle layer, while the remaining are due to the coupling of the lower two layers. As in the Elastic-Burgers-Maxwell model, the leading term (u_1) is separable in time and the deformation at the surface is not characterized by an exponential function (Fig. 18). In the models in Fig. 18, we set $h_1 = h_2$ and the ratio of Maxwell to Kelvin relaxation times identical in both layers. Hence, in these examples, the combination of the two Kelvin elements leads to a larger delayed elasticity, which is greater when the Kelvin element is weakest in the lower half-space (Fig. 18a). Furthermore, the distinction of the relaxation phases in the lower half-space is only apparent in the far-field when $\eta_{M3} < \eta_{M2}$ (Figs 18b–d). Finally, the deformation is better described by a logarithm than an exponential at distances less than about $10h_1$ (Fig. 18d). When $\eta_{M2} < \eta_{M3}$, because the dominant

transient deformation of the weakest Kelvin element is confined to the lower crust, the displacements can be characterized by either an exponential or logarithm far from the fault (Fig. 18e).

5 DISCUSSION

5.1 Phases of post-seismic relaxation

There are indeed multiple timescales in layered models with only Maxwell rheologies, but the surface displacements exhibit only one phase of post-seismic relaxation. When a weak Maxwell middle layer separates a faulted elastic layer from a Burgers viscoelastic lower region, the surface post-seismic displacements near the fault are shielded from the transient deformation of the Burgers rheology. The transient deformation due to the Kelvin element in the Burgers

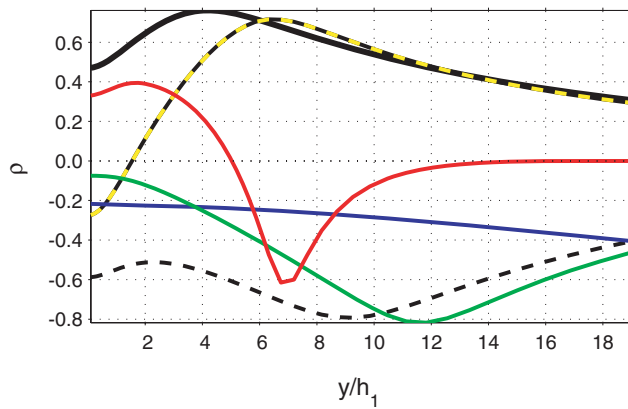


Figure 17. ρ with distance from the fault in an Elastic-Burgers model ($h_1 = h_2$; black solid line), an Elastic-Maxwell model (black dashed line), an Elastic-Maxwell-Burgers model ($\eta_{M2} = \eta_{M3}$; yellow and black dashed line) and for Elastic-Burgers-Maxwell models, with rheological properties and line colour as in Fig. 15.

rheology is only apparent at distances greater than about twice the thickness of the middle layer. On the other hand, when the middle Maxwell layer is stronger than the non-recoverable relaxation of the lower Burgers material, the surface displacements exhibit two phases of relaxation at all distances, with significant velocities of

deformation up to several tens of locking depths from the fault (i.e. long wavelength deformation). Alternatively, when a Burgers middle layer separates the upper elastic layer from a Maxwell viscoelastic lower region, there is pronounced transient surface deformation close to the fault, due to relaxation of the Kelvin element in the middle layer. Farther from the fault, a single phase of relaxation prevails, as the deformation is dominated by the Maxwell rheology of the lower half-space. That the surface displacements at increasing distances are dominated by relaxation at increasing depths, has been noted in several previous papers (e.g. Peltier 1974; Fang & Hager 1995; Piersanti *et al.* 1995; Pollitz 1997).

The surface post-seismic displacements always exhibit multiple phases of relaxation when there are two Burgers viscoelastic layers below a faulted elastic layer. Near the fault, the relaxation is similar to that of an Elastic-Burgers model regardless of the relative strengths of the non-recoverable components of relaxation between the layers. When the Maxwell relaxation time of the middle layer is greater than that of the lower region, the transient deformation is larger in the near field, and there is only one prominent phase of relaxation farther from the fault. On the other hand, when the steady component of deformation in the middle layer is stronger than the lower region, the transient deformation is larger farther from the fault.

Pollitz (2003) modelled the post-seismic deformation following the 1999 Hector Mine earthquake in southern California using a 3-D

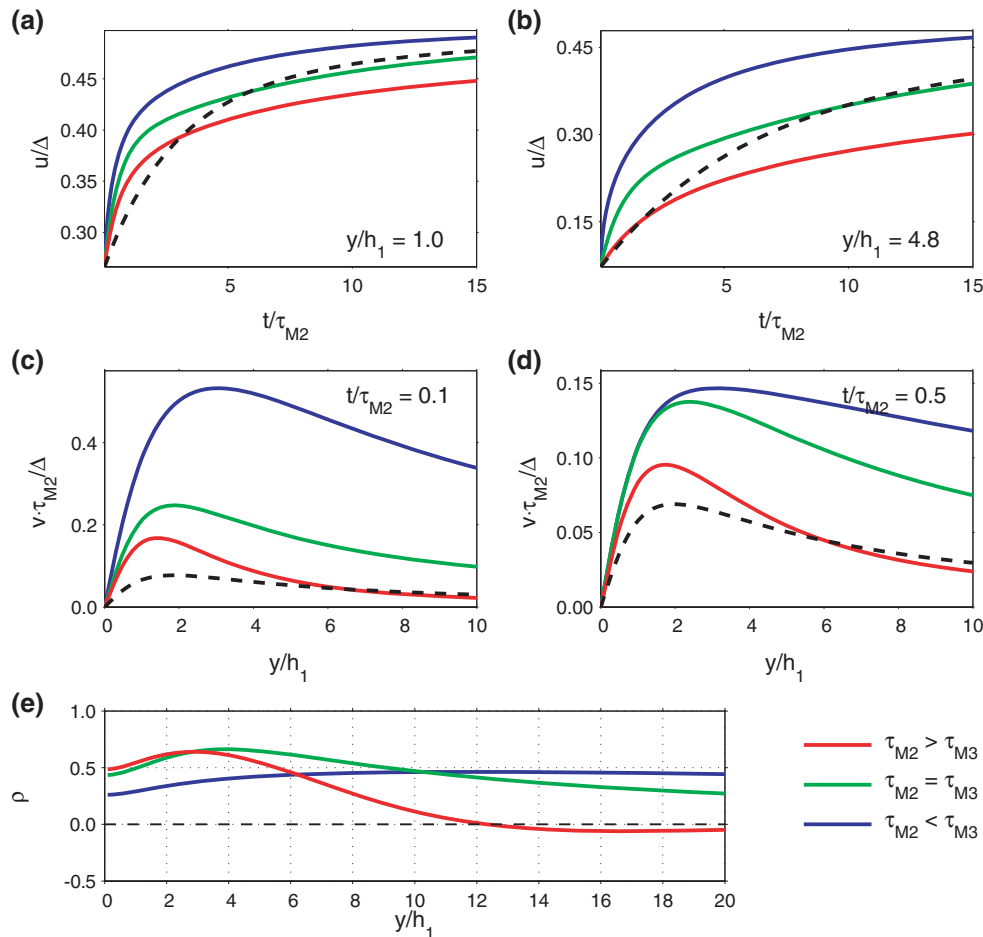


Figure 18. Post-seismic displacements (a) and (b), velocities (c) and (d) and ρ (e) for Elastic-Burgers-Burgers models ($h_1 = h_2$, $\mu_{Ki} = \mu_{Mi}/3$, and $\eta_{Ki} = 0.4\eta_{Mi}$ in both layers) with $\eta_{M3}/\eta_{M2} = 5.0$ (red), 1.0 (green), and 0.2 (blue). The displacements and velocities for an Elastic-Maxwell model are shown for reference (black dashed line).

model of a fault in an upper elastic layer over a Maxwell viscoelastic lower crust and a Burgers viscoelastic mantle. He found that the Maxwell relaxation time of the lower crust was much larger than that of the mantle, and determined relatively weak transient and steady viscous phase in the mantle ($\tau_{M2} \approx 2$ yr and $\tau_{K2} \approx 25$ days). In a 2-D model with such rheologies, the transient deformation would be significant up to 10 locking depths from the fault. When the finite length of the rupture is considered, the magnitude of the deformation is increasingly damped with distance from the fault (e.g. Hetland & Hager 2003), and in a 3-D model the deformation would not be nearly as large at great distance. Regardless, with a biviscous mantle separated from the elastic upper crust by a univiscous lower crust, the lower crust needs to be stronger than the mantle to predict the two phases of post-seismic relaxation observed within one locking depth of the Hector Mine rupture.

Models with lateral changes in rheology also produce multiple timescales. At a given location, the surface displacements depend on the material relaxation time of the material directly below, as well as the ratio of the relaxation times of the adjacent materials, expressed through lateral coupling coefficients. In some geometries, the surface post-seismic displacements above lateral transitions of rheologies may exhibit multiple phases. In the case when two univiscous materials are randomly distributed, the surface displacements do exhibit two phases of relaxation (Ivins & Sammis 1996). When a weaker Maxwell material is confined to zones whose width is of order, or greater, than the locking depth, the deformation only exhibits one relaxation phase (e.g. Pollitz 2001). The analytic solution for post-seismic deformation in models with laterally heterogeneous, albeit idealized, distributions of linear viscous rheologies follows directly from the theory of Hetland & Hager (2005), and is a topic of ongoing research.

5.2 Possible physical interpretation of Kelvin viscoelasticity

Logarithmic functional forms have been proposed to describe low temperature creep (Lomnitz 1956), as well as post-seismic deformation due to frictional after-slip (Marone *et al.* 1991). That post-seismic displacements at the surface due to stress relaxation in a Burgers viscoelastic material can be parametrized by a logarithm indicates that inferences of either post-seismic after-slip or Burgers viscoelastic relaxation may be non-unique. However, consideration of all three components of deformation in 3-D models may resolve the non-uniqueness (e.g. Hearn 2003; Pollitz 2003). The Kelvin element is used to describe time dependent grain boundary sliding in response to the stresses due to seismic wave propagation (e.g. Jackson *et al.* 2002), and it has been noted that relaxation times within the absorption band of Earth can be up to several decades (e.g. Anderson & Given 1982). On a crustal scale, the transient Kelvin deformation may be an analogue for grain readjustment and distributed slip in the frictional-viscous transition region observed at the base of exhumed faults (e.g. Stewart *et al.* 2000). Finally, the initial transient deformation of the Burgers rheology may be a proxy for low temperature creep (e.g. Pollitz 2005; Savage *et al.* 2005). The transient deformation in the Burgers rheology is recoverable, and while seismic studies assume that the transient rock deformation is completely recoverable, distributed after-slip is likely not fully recoverable.

5.3 Implications for interseismic deformation

The 2-D model of Savage & Prescott (1978), has been used to make inferences of the rheology of the continental lithosphere (e.g. Segall

2002; Hilley *et al.* 2005; Meade & Hager 2005). The model of Savage & Prescott (1978) is of repeated ruptures on a fault in an elastic layer over a Maxwell viscoelastic half-space, and thus the estimate of the viscosity of the lithosphere that comes out of this one-layer model is an effective viscosity, which depends on the rheologies of the entire lithosphere. The mapping of the rheological parameters in one-layer models, with repeated earthquakes, to those in multiple layer models is beyond the scope of this paper, but a rough estimation can be made from the illustrations we present.

When the middle layer is weaker than the lower half-space, the apparent Maxwell relaxation time in the one-layer model is roughly one and a half to two times that of the Maxwell relaxation time of the middle layer. Additionally, the deformation is more concentrated near the fault in two-layer models, and thus the deformation throughout a seismic cycle would require a smaller locking depth in one-layer models. On the other hand, when the lower region is weaker than the middle layer, the apparent Maxwell relaxation time of the one-layer model is about one-half that of the middle layer; additionally the deformation is of longer wavelength, requiring a larger locking depth in the one-layer models.

Hilley *et al.* (2005) estimated a viscosity of 10^{19} – 10^{21} Pa-sec by fitting the one-layer model of Savage & Prescott (1978) to the interseismic deformation across the Kunlun fault in Tibet. Assuming that the mantle lithosphere is much stronger than the lower crust under Tibet, they argued that the half-space viscosity represents the viscosity of the lower crust. To justify this inference of the strengths of the lower crust and mantle, they referenced one of our previous papers (Hetland & Hager 2004). While we did indeed demonstrate that post-seismic relaxation in the presence of a weak lower crust is dominated by the relaxation in that layer (by no means a novel contribution), we did not address the mapping between the viscosity in a one-layer model to those in a two-layer model. If the mantle lithosphere is stronger than the lower crust, the deformation in Tibet would be much shorter wavelength than a one-layer model, and thus the locking depth of the one-layer model would need to be shallower than the actual. If the locking depth Hilley *et al.* (2005) estimated is appropriate for the Kunlun fault, it may indicate that a one-layer model is a good approximation to the lithosphere under Tibet, and that the strengths of the mantle lithosphere and lower crust are not greatly different. However, strains across the fault are greater early in the seismic cycle and lower late in the cycle, and the apparent locking depth of an equivalent elastic model increases throughout the seismic cycle (e.g. Savage & Lisowski 1998; Hetland & Hager 2006). Hence, there is a trade-off between locking depth and time within the seismic cycle, and if the mantle is much stronger than the lower crust, Hilley *et al.* (2005) may have inferred that the Kunlun fault is later in the cycle than it is. Finally, as noted by Hilley *et al.* (2005), the data they studied are located to the west of a recent large rupture on the Kunlun fault, and neglecting 3-D effects of the fault ruptures may bias their findings. The study of Hilley *et al.* (2005) is an excellent illustration that a large parameter space can be rigorously explored using computationally cheap models that overly simplify the geometry and rheology of the lithosphere. However, to accurately draw inferences of the parameters in more complex models, the mapping between the models needs to be addressed.

6 CONCLUSIONS

In this paper we examine post-seismic deformation in models of an elastic layer over a viscoelastic layer and a viscoelastic half-space. To fundamentally understand deformation in layered models, we

generalize the theory of Hetland & Hager (2005) from one layer over a half-space to two layers over a half-space. We also use finite element models to demonstrate the differences between models with one and two layers over a half-space. We consider both univiscous Maxwell rheologies and biviscous Burgers rheologies. In layered viscoelastic models, there are multiple mechanical timescales of the post-seismic deformation. However, not all of these times arise as distinct phases of post-seismic relaxation observed at the surface. The surface displacements in layered models with only univiscous, Maxwell viscoelastic rheologies always exhibit one phase of relaxation. Layered models containing biviscous rheologies may produce multiple phases of relaxation; however, the relative strengths of the layers, in addition to the number of viscous phases in each layer, affect the distinctness of the phases of surface deformation. In the case when a faulted elastic layer is directly over a multiviscous rheology, multiple phases of relaxation are always visible near the fault, and the post-seismic displacements can be often described by a logarithmic function.

ACKNOWLEDGMENTS

Reviews by the Editor, Dr J. Beavan, and two anonymous reviewers greatly improved this paper. We thank K.J. Bathe and Adina R&D, Inc. for the use of Adina. This research was supported by NSF grant EAR-0346021.

REFERENCES

- Anderson, D.L. & Given, J.W., 1982. Absorption band Q model for the Earth, *J. geophys. Res.*, **87**, 3893–3904.
- Burgers, J.M., 1939. Mechanical considerations—model systems—phenomenological theories of relaxation and of viscosity, in *First Report on Viscosity and Plasticity*, pp. 5–72, prepared by the committee for the study of viscosity of the Academy of Sciences at Amsterdam, Nordmann Publishing Company, Inc., New York.
- Carter, N.L. & Ave'Lallemant, H.G., 1970. High temperature flow of dunite and peridotite, *Geol. Soc. of Am. Bull.*, **81**, 2181–2202.
- Chinnery, M.A., 1961. Deformation of the ground around surface faults, *Bull. seism. Soc. Am.*, **51**, 355–372.
- Chinnery, M.A. & Jovanovich, D.B., 1972. Effect of Earth layering on earthquake displacement fields, *Bull. seism. Soc. Am.*, **62**, 1629–1639.
- Churchill, R.V., 1944. *Modern Operational Mathematics in Engineering*, 306 pp., McGraw-Hill Book Company Inc., New York.
- Fang, M. & Hager, B.H., 1995. The singularity mystery associated with a radially continuous Maxwell viscoelastic structure, *Geophys. J. Int.*, **123**, 849–865.
- Findley, W.N., Lai, J.S. & Onaran, K., 1976. *Creep and Relaxation of Nonlinear Viscoelastic Materials: With an Introduction to Linear Viscoelasticity*, 371 p., Dover Publications, New York.
- Flügge, W., 1967. *Viscoelasticity*, 119 p., Blaisdell Publishing Company, Waltham, Massachusetts.
- Freed, A.M. & Bürgmann, R., 2004. Evidence of power-law flow in the Mojave desert mantle, *Nature*, **430**, 548–551.
- Hager, B.H., Lyzenga, G.A., Donnellan, A. & Dong, D., 1999. Reconciling rapid strain accumulation with deep seismogenic fault planes in the Ventura basin, California, *J. geophys. Res.*, **104**, 25 207–25 219.
- Hearn, E.H., 2003. What can GPS data tell us about the dynamics of post-seismic deformation?, *Geophys. J. Int.*, **155**, 753–777.
- Hearn, E.H. & Bürgmann, R., 2005. The effects of elastic layering on inversion of GPS data for coseismic slip and resulting stress changes: strike-slip earthquakes, *Bull. Seism. Soc. Am.*, **95**, 1637–1653.
- Herring, T.A., 2003. Results and comparisons from the Southern California Integrated and other arrays, *EOS, Trans. Am. geophys. Un.*, **85**, Fall Meet. Suppl., Abstract G32B-04.
- Hetland, E.A. & Hager, B.H., 2003. Postseismic relaxation across the Central Nevada Seismic Belt, *J. geophys. Res.*, **108**(B8), 2394, doi:10.1029/2002JB002257.
- Hetland, E.A. & Hager, B.H., 2004. Relationship of Geodetic Velocities to Velocities in the Mantle, *Geophys. Res. Lett.*, **31**, L17604, doi:10.1029/2004-Gl020691.
- Hetland, E.A. & Hager, B.H., 2005. Postseismic and interseismic displacements near a strike-slip fault: a 2D theory for general linear viscoelastic rheologies, *J. geophys. Res.*, **110**, B10401, doi:10.1029/2005JB003689.
- Hetland, E.A. & Hager, B.H., 2006. Interseismic deformation: cycle invariance, slip-rate, and rheology, *Geochem. Geophys. Geosyst.*, in press.
- Hilley, G.E., Bürgmann, R., Zhang, P.Z. & Molnar, P., 2005. Bayesian inference of plastosphere viscosities near the Kunlun Fault, northern Tibet, *Geophys. Res. Lett.*, **32**, L01302, doi:10.1029/2004GL021658.
- Ivins, E.R., 1996. Transient creep of a composite lower crust; 2, a polymineralic basis for rapidly evolving postseismic deformation modes, *J. geophys. Res.*, **101**, 28 005–28 028.
- Ivins, E.R. & Sammis, C.G., 1996. Transient creep of a composite lower crust; 1, Constitutive theory, *J. geophys. Res., B. Solid Earth and Planets*, **101**, 27 981–28 004.
- Jackson, I., Fitz, J.D., Faul, U.H. & Tan, B.H., 2002. Grain-size-sensitive seismic wave attenuation in polycrystalline olivine, *J. geophys. Res.*, **107**(B12), 2360, doi:10.1029/2000JB001225.
- Kohlstedt, D.L., Evans, B. & Mackwell, S.J., 1995. Strength of the lithosphere: constraints imposed by laboratory experiments, *J. geophys. Res.*, **100**, 17 587–17 602.
- Lomnitz, C., 1956. Creep measurements in igneous rocks, *J. Geol.*, **64**, 473–479.
- Lyzenga, G.A., Raefsky, A. & Mulligan, S.G., 1991. Models of recurrent strike-slip earthquake cycles and the state of crustal stress, *J. geophys. Res.*, **96**, 21 623–21 640.
- Marone, C.J., Scholz, C.H. & Bilham, R., 1991. On the mechanics of earthquake afterslip, *J. geophys. Res.*, **96**, 8441–8452.
- Meade, B.J. & Hager, B.H., 2005. Block models of crustal motion in southern California constrained by GPS measurements, *J. geophys. Res.*, **110**, B03403, doi:10.1029/2004JB003209.
- Montési, L.G.J., 2004. Controls of shear zone rheology and tectonic loading on postseismic creep, *J. geophys. Res.*, **109**, B10404, doi:10.1029/2003JB002925.
- Nur, A. & Mavko, G., 1974. Postseismic viscoelastic rebound, *Science*, **183**, 204–206.
- Peltier, W.R., 1974. The impulse response of a Maxwell Earth, *Rev. Geophys. Space Phys.*, **0**, 649–669.
- Piersanti, A., Spada, G., Sabadini, R. & Bonafede, M., 1995. Global post-seismic deformation, *Geophys. J. Int.*, **120**, 544–566.
- Pollitz, F.F., 1997. Gravitational viscoelastic postseismic relaxation on a layered spherical Earth, *J. geophys. Res.*, **102**, 17 921–17 941.
- Pollitz, F.F., 2001. Viscoelastic shear zone model of a strike-slip earthquake cycle, *J. geophys. Res.*, **106**, 26 541–26 560.
- Pollitz, F.F., 2003. Transient rheology of the uppermost mantle beneath the Mojave Desert, California, *Earth planet Sci. Lett.*, **215**, 89–104.
- Pollitz, F.F., 2005. Transient rheology of the upper mantle beneath central Alaska inferred from the crustal velocity field following the 2002 Denali earthquake, *J. geophys. Res.*, **110**, B08407, doi:10.1029/2005JB003672.
- Roberts, G.E. & Kaufman, H., 1966. *Table of Laplace Transforms*, 137 p., WB Saunders Co., Philadelphia.
- Rundle, J.B. & Jackson, D.D., 1977. A three-dimensional viscoelastic model of a strike slip fault, *Geophys. J. R. astr. Soc.*, **49**, 575–591.
- Rutter, E.H. & Brodie, K.H., 1992. *Rheology of the lower crust*, 201 pp., Elsevier, New York.
- Rybicki, K., 1971. The elastic residual field of a very long strike-slip fault in the presence of a discontinuity, *Bull. seism. Soc. Am.*, **61**, 79–92.
- Savage, J.C., 1987. Effect of crustal layering upon dislocation modeling, *J. geophys. Res.*, **92**, 10 595–10 600.
- Savage, J.C., 2000. Viscoelastic-coupling model for the earthquake cycle driven from below, *J. geophys. Res.*, **105**, 25 525–25 532.

- Savage, J.C. & Lisowski, M., 1998. Viscoelastic coupling model of the San Andreas Fault along the big bend, Southern California, *J. geophys. Res.*, **103**, 7281–7292.
- Savage, J.C. & Prescott, W.H., 1978. Asthenosphere readjustment and the earthquake cycle, *J. geophys. Res.*, **83**, 3369–3376.
- Savage, J.M., Svarc, J.L. & Prescott, W.H., 2003. Near-field post-seismic deformation associated with the 1992 Landers and 1999 Hector Mine, California, earthquakes, *J. geophys. Res.*, **108**(B9), 2432, doi:10.1029/2002JB002330.
- Savage, J.C., Svarc, J.L. & Yu, S.B., 2005. Postseismic relaxation and transient creep, *J. geophys. Res.*, **110**, B11402, doi:10.1029/2005JB003687.
- Segall, P., 2002. Integrating geologic and geodetic estimates of slip rate on the San Andreas fault system, *Int. Geol. Rev.*, **44**, 62–82.
- Smith, B. & Sandwell, D., 2004. A three-dimensional semianalytic viscoelastic model for time-dependent analysis of the earthquake cycle, *J. geophys. Res.*, **109**, B12401, doi:10.1029/2004JB003185.
- Stewart, M., Holdsworth, R.E. & Strachan, R.A., 2000. Deformation processes and weakening mechanisms within the frictional-viscous transition zone of major crustal-scale faults: insights from the Great Glen Fault Zone, Scotland, *J. Struct. Geol.*, **22**, 543–560.
- Weertman, J. & Weertman, J.R., 1964. *Elementary Dislocation Theory*, 213 pp., Macmillan, New York.